2023

A Study of the Influence of Heat Flux on Aerodynamics in Hypersonic Flow

Kristina Pionessa
University of Central Florida

A STUDY OF THE INFLUENCE OF HEAT FLUX ON AERODYNAMICS IN HYPERSONIC FLOW

by

KRISTINA RACHEL PIONESSA
B.S University of Central Florida, 2021

A thesis submitted in partial fulfillment of the requirements
for the degree of Master of Science in Aerospace Engineering
in the Department of Mechanical and Aerospace Engineering
in the College of Engineering and Computer Science
at the University of Central Florida
Orlando, Florida

Summer Term
2023

Major Professor: Michael P. Kinzel

ABSTRACT

This study investigates the utilization of computational fluid dynamics (CFD) to simulate aerodynamic heating effects in support of research and design endeavors. The initial investigation demonstrates the effectiveness of a computational approach in analyzing different geometries and flow conditions. Specifically, CFD is employed to analyze the aerodynamics of a blunt cone, double cone, and hypersonic leading edge experiencing a changing heat source across the flow/body boundary. At the stagnation point, maximum thermal loading occurs as previously found; therefore, boundary layer thickness and shock standoff distance is measured at that position to compare the results of each case. Characteristics such as temperature and pressure reveal shock and boundary layer distance and how the heat flux shifts the layers away from the body as its added into flow, and narrows the regions as the flow is cooled. For the more complex geometry of the double cone, two shocks are seen in adiabatic flow, but increasing heat flux into the flow pushes the shock layer further from the body until the shocks merge, causing drag reduction across the body; simulating an ablative heat shield that is burning. Overall, designs of a simpler nature are less influenced by heat flux, but more complex designs and regions demand considering heat flux, or even use it to an aerodynamic design advantage.

ACKNOWLEDGEMENTS

Thank you to my graduate advisor, Dr. Michael Kinzel, for all the support and guidance provided throughout my graduate studies. I also want to thank my fellow graduate students in the Computational Fluids and Aerodynamics Lab; I couldn't have done this without your professional collaboration or friendship. Finally, thank you to my family, for I truly couldn't have made it this far without your unwavering support and encouragement.

TABLE OF CONTENTS

LIST OF FIGURES

LIST OF TABLES

CHAPTER 1: INTRODUCTION

Hypersonic weapons have seen major technological developments in recent decades and will continue to be a focus in those that follow. Although different than space exploration, these weapons face similar issues for design and analysis. There are simple models that predict heat transfer for axisymmetric bodies, such as simple cylindrical missile bodies or cones, at zero angle of attack; however, when additional features such as stabilizing devices (fins and flares), aerodynamic surfaces for lateral acceleration, control jets, or deviations from axial symmetry are introduced, the predictions become more complex. Flow separations and reattachments become influential to overall flow. Predicting heat transfer in such flow regions becomes challenging, especially when the boundary layer is no longer laminar, but transitional or turbulent. These flow regions can experience substantial increases in heat transfer [1].

Aerocapture is a technique used in space exploration that utilizes the atmosphere of a planet or moon, to slow down a spacecraft before entry, descent, and landing (EDL). As indicated along the red line with numbers in the diagram Figure 1, the spacecraft (1) approaches its targeted body and (2) passes through the upper atmosphere. Through steps (2)-(6) atmospheric drag is used to slow the vehicle speed, it then (7) returns to space where after steps (2)-(7) are repeated[2]. The entry events and corresponding drag on the spacecraft drive changes to the entry trajectory, and each time the space craft passes through the atmosphere it does so for a longer duration until the craft reaches the velocity and orbit necessary to initiate EDL. These recurring entry events are particularly useful for missions that require precise orbital insertion or when the spacecraft needs to conserve propellant[2]. Propellant conservation allows the mission to withstand a greater payload or allow for the propellant to be used for longer mission range compared to the amount that would be required to safely slow a spacecraft before EDL.

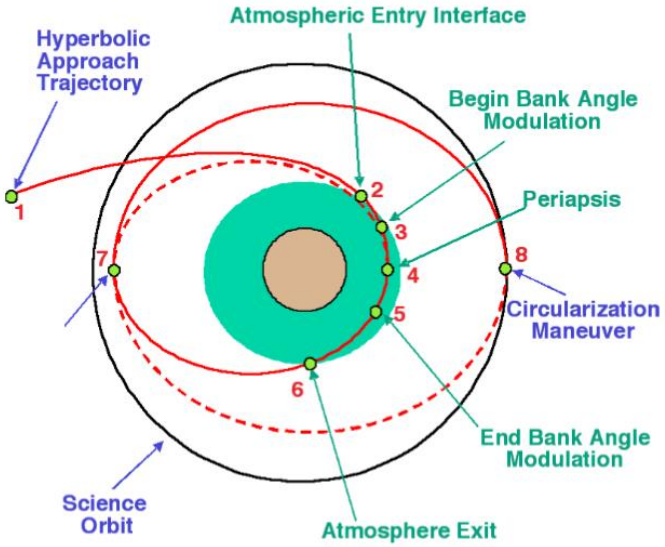

Figure 1: Aerocapture flight schematic [3]

When a spacecraft enters an atmosphere during the entry phase, the flow is typically in hypersonic conditions (i.e., Mach 5 or greater). In such conditions, the vehicle experiences challenges associated with low atmospheric density, sharp changes in the primitive flow variables (p, T, ρ), and corresponding complexities associated with aerodynamic forces and extreme heating[4]. These sharp changes in the flow variables are tied to shocks forming in high-speed flow fields that are specifically critical. When a flow encounters a shock wave, it undergoes a sudden compression and deceleration. The pressure behind the shock wave is significantly higher than the pressure ahead of it, which generates aerodynamic forces, including drag and lift, which can affect the stability and control of objects in high-speed flows. This disruption can lead to flow separation that negatively impacts aerodynamic performance, stability, and control. The compression of the flow increases molecule collisions, kinetic energy, and frictional drag, leading to higher heat transfer. Understanding and accounting for the effects of shock waves are crucial in the design and operation of high-speed vehicles and spacecraft.

Engineers employ various techniques, such as computational fluid dynamics (CFD) simulations and wind tunnel testing, to analyze and mitigate the impacts of shock waves on aerodynamics, heat transfer, and structural considerations. As an aerocapture maneuver is driven by drag force, the shock and heat transfer effects must be fully understood. Experimentation within high-speed flows is costly and difficult to execute, so CFD provides engineers an opportunity to analyze design in a less expensive and repeatable way. Understanding and accounting for the effects of shock waves are crucial in the design and operation of high-speed spacecraft and weapons. Expanding our understanding of how hypersonic flow is affected by heat transfer reveals relationships of heat transfer and shock characteristics. As shock relations have been previously explored for axisymmetric, zero angle of attack cases, those cases are utilized in this study to isolate heat flux in and out of flow at a body's surface, allowing us to see its impact on CFD simulations.

CHAPTER 2: BACKGROUND

2.1 Hypersonic Flow Overview

Supersonic flow is defined as speeds between Mach 1.2 to 4.9, while hypersonic flow is defined as anything faster than Mach 5. For both flow regimes, shock waves form as flow compresses over a body, nearly causing discontinuities in the flow. Hypersonic flows can be explained by the same flow relations as supersonic flows, but vary as the physical phenomena are more impactful with increasing Mach number. Differences in shock characteristics, entropy layer, effects of viscosity, temperature, and density lead to shock-viscous-layer interactions and dissociation highlighted below[4].

Hypersonic shocks have a thinner shock layer, (smaller shock stand-off distance) as the density jump across the shock increases[5]. This is prevalently seen with blunt bodies experiencing high backpressure downstream. The flow experiences increasing boundary layer thickness; therefore, the shock and boundary layer start to merge, creating a physically complex flow regime. Passing through a shock wave results in an increase in entropy, which represents the level of disorder in the flow. A more intense shock wave produces a greater increase in entropy. For a curved shock wave, near the flow's centerline (or the axis in axisymmetric bodies) the shock experiences a higher entropy increase compared to the streamline passing further from the centerline where the shock is generally weaker. The boundary layer that develops on the surface of an object expands within the entropy layer and experiences vorticity interaction[4].

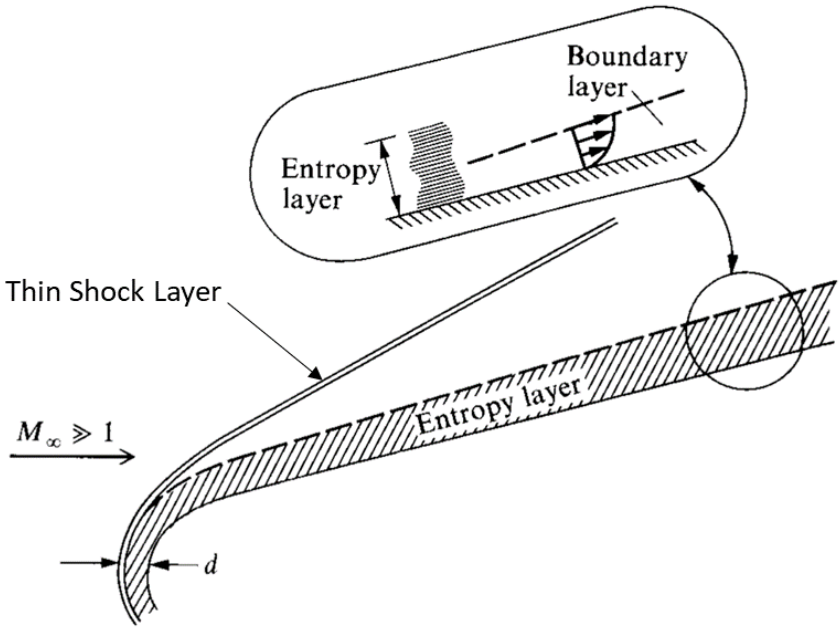

Figure 2: Hypersonic thin shock layer and entropy layer [4]

Viscous dissipation occurs in hypersonic flow as viscosity transforms kinetic energy in the flow to internal energy within the boundary layer. With internal energy increasing, the boundary layer sees an increase in temperature; therefore, the boundary layer increases in thickness, $\delta \propto \frac{M_\infty^2}{\sqrt{Re_x}}$, and a correlating decrease in density from ideal gas, $\rho = p/RT$[4]. The thick boundary layer has a significant influence on the flow outside of it, affecting the growth of the boundary layer itself and causing a body shape to appear thicker than its actual dimensions. Viscous interactions between the boundary layer and inviscid flow beyond play a crucial role in determining the surface-pressure distribution, lift, drag, and stability of hypersonic vehicles; in addition, skin friction and heat transfer are intensified. Due to the viscous interaction, the pressure near the nose of a body is significantly higher, and the surface-pressure distribution gradually decreases downstream. Eventually the pressure approaches a downstream value equivalent to that of an inviscid flow. This highlights the importance of shock-viscous-layer interactions for the nose region only. In some cases, the boundary layer on a hypersonic vehicle becomes so thick that it

merges with the shock wave, forming a merged shock layer. When this occurs, the shock layer must be treated as fully viscous, and the conventional boundary-layer analysis is no longer applicable [4].

In hypersonic flows, the dissipation of kinetic energy occurs through friction within the boundary layer increasing temperature as explained above. These temperatures are sufficient to excite internal molecular vibrations, cause ionization, and induce dissociation within the flow. As vehicles are protected with ablative heat shields, or various coatings, such as an oxidizing chromium, the surface of a hypersonic vehicle being affected by a chemically reacting boundary layer. The key impact is a change of heat flux in/out of the vehicle surface affecting the characteristics of the boundary layer and shock layer. In addition, there is another region of high-temperature flow over a hypersonic vehicle. In the nose region of a blunt cone, the bow shock wave is either normal or close to being normal to the flow direction. Behind this shock wave, temperatures can reach extremely high levels in hypersonic flows. The entire shock layer can also be dominated by chemically reacting flow. At high gas temperatures, the gas deviates from this ideal behavior and exhibits "nonideal" characteristics considering the vibrational energy change, and presence of chemical reactions as explained above[4].

2.2 Previous Studies

2.2.1 Maximum Thermal Loading

A study was conducted for the characterization of multilayered ceramic composite systems in hypersonic flow[6]. As hypersonic flights face thermal strain and chemical reactions between the solid and fluid regions, failure of the materials is likely to take place. In order to understand these failures greater, a two-dimensional CFD model was developed to analyze heat generation

and transfer within a material system subjected to hypersonic flow. The material geometry and fluid domain mesh were defined, utilizing the geometry and meshing for separate regions, for conjugate heat transfer analysis. The solid body had the defined materials and thickness as follows: TiAlN 40 µm, Ti 50 µm, Al_2O_3 500 µm, Binder 30 µm, and IN738 3000 µm. The geometry of the leading-edge has a 1 mm radius, 5-degree offset and 152 mm chord length. Initial conditions within the fluid domain simulated Mach 5 conditions with specific air properties, with solid regions initialized at 300 K, and the inner boundary of the IN738 layer matched experimental ambient temperatures. The study focused on determining the maximum thermal loading. This was determined at the stagnation point on the leading-edge during level flight, or 0 angle of attack, as shown in Figure ***3*** [6].

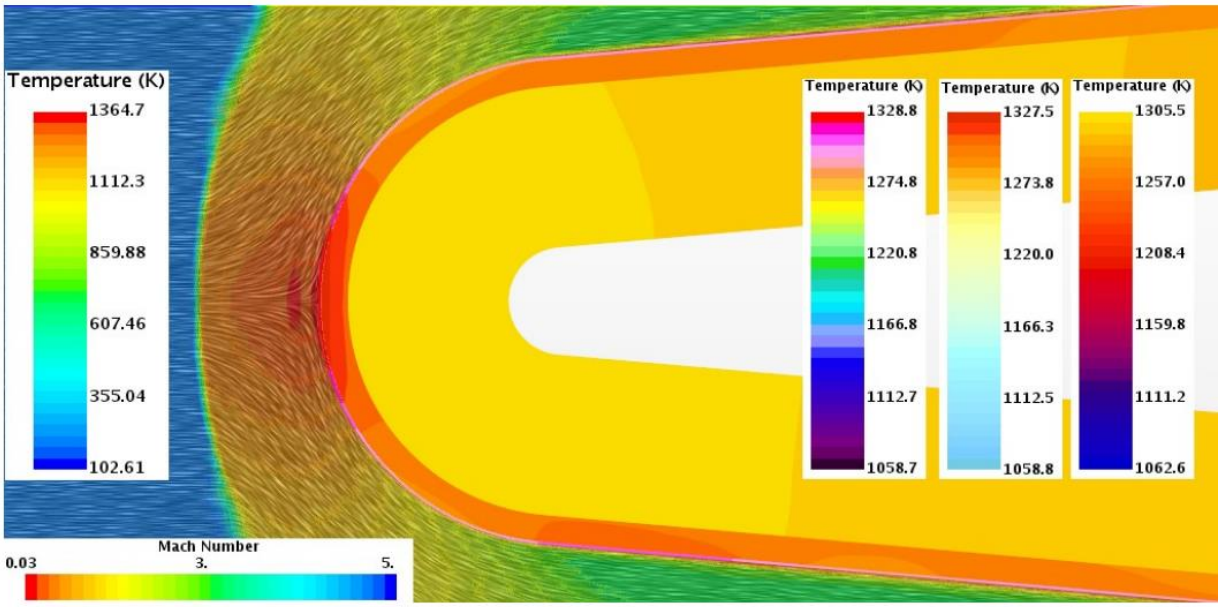

Figure 3: 2D temperature contour at blunt 1 mm radius leading edge [6]

2.2.2 Aerothermal Effects of Heat Release in Hypersonic Shock Layers

Deep and Jagadeesh conducted a study that examined the effects of controlled heat addition into the chemically reacting shock layer of a large angle blunt cone with a spherical nose[5]. Their study utilized hypersonic experimentation involving the exothermic oxidation of ablated chromium from a cone's surface at hypersonic Mach numbers, with a free-stream Mach 9.84 [5]. A test model consisting of a conical skirt was used. The experiments measured temperature distribution in the shock layer using two-color ratio pyrometry and a DSLR camera as a pyrometer. Surface heat flux measurements were obtained using calibrated thin film platinum heat transfer gauges. The experiments also focused on measuring shock stand-off distances through Schlieren imaging and a new intensity-scan based method. For the same geometry, the experiment was conducted for an aluminum cone, and one coated with 10 μm thick chromium. The calculations showed a rise in gas temperature of 173 K in the stagnation region due to chromium oxidation, accompanied by an increase in net surface heat flux of about 31 W/cm2, and the measured shock stand-off distance increased by approximately 17%.

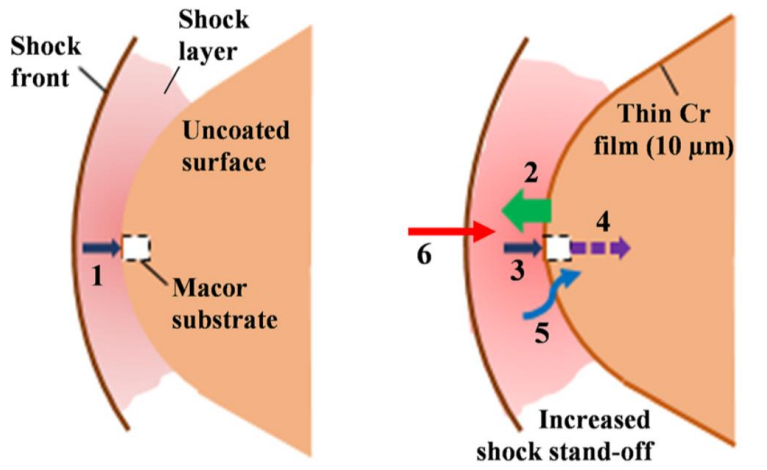

1 Convective heat flux at stag. pt. (uncoated)= 122.11 W/cm^2
2 Heat released due to Cr oxidation (H)= 78 W/cm^2
3 Convective total heat flux at stag. pt. with Cr coating= 153.34 W/cm^2
4 Heat loss from Macor rear by conduction= 0.31 W/cm^2
5 Radiative heat flux near stag. pt.= 6.2 W/cm^2
6 Heat used up in raising shock layer temp.= 1.5 W/cm^2
Heat pushing shock layer away from surface (Δh) = 2-(3-1)-4-5-6= 78-(153.34-122.11)-0.31-6.2-1.5 ~ 39 W/cm2

Figure 4: Chromium oxidization kinetics – distribution of released heat due to exothermic oxidization of Cr [5]

Analytical calculations displaying chromium oxidation kinetics shown in Figure *4* display that the total exothermic heat release was distributed into various processes. About 78 W/cm2 of energy released in the stagnation region of the shock layer; in conclusion, this energy was broken into 1.9% increased the temperature of the gas layer, 40% convected back into the airframe, 0.4% lost through conduction from the rear of the substrate, and around 8% radiated into the model. The remaining 50% of the heat was utilized to push the shock layer away from the body, increasing the shock stand-off distance by raising its density [5]. This study brings up the question of what characteristics within the shock layer are influenced by the heat flux into the flow, and what predictions can be used for the future of hypersonic cooling design.

2.2.3 Simulating Hypersonic Flows

Conducting hypersonic experiments pose several challenges associated with complexity and costs. In these scenarios, engineers conduct wind tunnel tests which can have error associated with controlling the flow and instrumenting models; they are also time consuming to prepare, and are costly due to limiting error and providing enough power for hypersonic free-stream velocities. When in early phase of designs or studies, cost, time, and accuracy are important factors that require an alternative to physical experimentation. This is where CFD comes in. Utilizing in house computational codes, and even commercials, provide essential insight as analysis progresses. One such commercials code, STAR-CCM+ , is utilized within academia and industry [7]. Cross and West investigated the accuracy of STAR-CCM+ compared to wind tunnel testing for the use of hypersonic flow fields utilizing multiple geometries that experienced a wide variety of flow conditions.

For a double cone geometry, experimental runs occurred for flow nitrogen and air, but we will focus on the air model. Air models were run for single species air, and multiple species with reacting and non-reacting models. As seen in Figure *5*, the single species air model observed lower temperatures than the chemically reactive cases as the assumes the vibrational relaxation and chemical reaction processes are infinitely fast [8]. When feasible, accurately simulating the air composition and reaction leads to higher accuracy in CFD results, but the simplified model (equilibrium air) is comparable to experimentation for early phase design iterations.

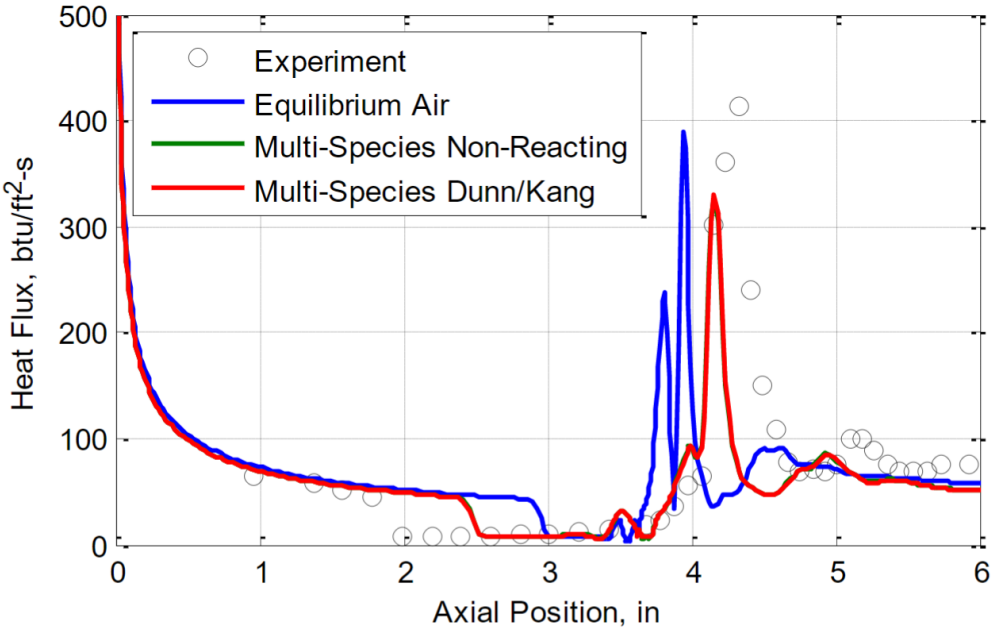

Figure 5: Comparison of heat flux as predicted by different simulations [8]

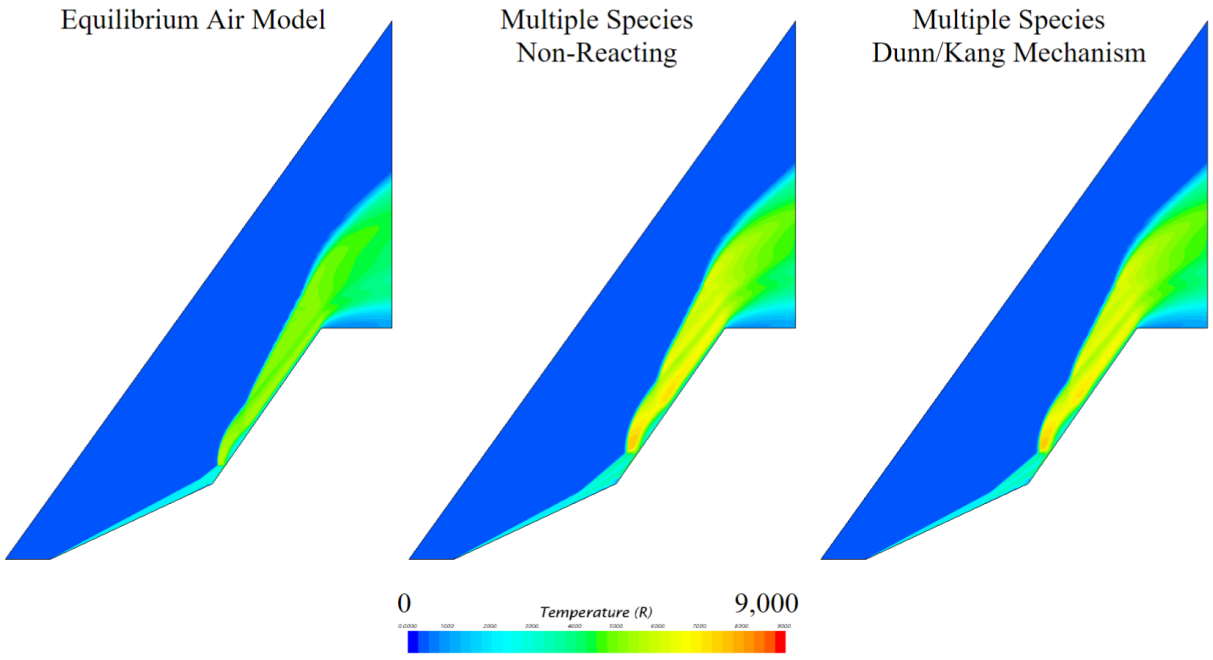

Figure 6: Comparison of temperature distribution as predicted by different simulations for double cone air run [8]

CHAPTER 3: METHODS

3.1 Governing Equations

3.1.1 Reynolds-Averaged Navier Stokes Equations

To define the basis of underlying fluid flow, a set of partial differential equations are used, the Navier Stokes equations. The equation is defined as the conservation of mass, momentum, and energy transport, respectively [7]. The continuity equation is defined by the mass flow through a control volume with density, ρ, over and flow velocity, v,

$$\frac{\partial \rho}{\partial t} + \nabla \cdot (\rho \vec{v}) = 0 \tag{1}$$

The conservation of momentum is defined as

$$\frac{\partial (\rho \vec{v})}{\partial t} + \nabla \cdot (\rho \vec{v} \vec{v}) = -\nabla P + \nabla \cdot \left(\overline{\overline{\tau}}\right) + \rho \vec{g} + \vec{F} \tag{2}$$

with the identity matrix, I, the body force, $\overrightarrow{F}$, and the defined stress tensor,

$$\overline{\overline{\tau}} = \mu \left[\left(\nabla \vec{v} + \nabla \overrightarrow{v^{T}} \right) - \frac{2}{3} \nabla \cdot \vec{v} I \right] \tag{3}$$

Utilizing the velocity and the viscosity, μ. Similarly, the energy transport equation is defined as

$$\frac{\partial(\rho E)}{\partial t} + \nabla \cdot \left[\vec{V}(\rho E + p)\right] = \nabla \cdot \left[k_{eff}\nabla T - \sum_j h_j J_j + \left(\bar{\bar{\tau}}_{eff} \cdot \vec{V}\right)\right] + S_h$$

(4)

where E is the total energy.

3.1.2 Hypersonic Shock Relations

The exact shock relations derived in supersonic aerodynamics remain valid in hypersonic speeds without any changes; however, at high Mach number limit (approaching infinity), approximate forms of these shock relations can be derived. The exact calculations are used to eliminate oversimplification. Below are the oblique shock relations with the assumption that constant specific heats apply for $\gamma = \frac{c_p}{c_v}$. For all equations, upstream and downstream are denoted by subscripts 1 and 2 respectively. Additionally, β is the wave angle of the oblique shock and M_1 is the free stream Mach. The ratios of properties before and after the shock are below [4].

Pressure ratio:

$$\frac{p_2}{p_1} = 1 + \frac{2\gamma}{\gamma + 1}(M_1^2 \sin^2 \beta - 1)$$

(5)

Density ratio:

$$\frac{\rho_2}{\rho_1} = \frac{(\gamma + 1)M_1^2 \sin^2 \beta}{(\gamma - 1)M_1^2 \sin^2 \beta + 2}$$

(6)

Ideal gas equation of state ($p = \rho R\, T$) is used to simply temperature ratio to:

$$\frac{T_2}{T_1} = \frac{(p_2/p_1)}{(\rho_2/\rho_1)}$$

(7)

The free stream velocity is broken up into the x and y coordinates (u and v respectively) behind the shock wave. They create a total deflection angle of θ for the flow rotating from the initial velocity to the downstream velocity.

$$\frac{u_2}{V_1} = 1 - \frac{2(M_1^2 \sin^2 \beta - 1)}{(\gamma + 1)M_1^2}$$

(8)

$$\frac{v_2}{V_1} = \frac{2(M_1^2 \sin^2 \beta - 1)\cos \beta}{(\gamma + 1)M_1^2}$$

(9)

Pressure coefficient, C_p, is used to nondimensionalize the pressure value by utilizing the dynamic pressure, q_1.

$$C_p = \frac{p_2 - p_1}{q_1} = \frac{2}{\gamma M_1^2}\left(\frac{p_2}{p_1} - 1\right)$$

(10)

3.1.3 Aerodynamic Heating

Aerodynamic heating occurs through the compression of the flow through shocks shown above. Additionally, viscous effects occur through skin friction and surface heat transfer is produced, being heavily influential to the flow field. Stanton number, C_H, is the dimensionless ratio of heat transfer in flow to the flow's thermal capacity. Simplified form of a flat plate enthalpy, h, at the wall and adiabatic conditions, and u_e, the velocity at the edge of the boundary layer.

$$C_H = \frac{q_w}{\rho_e u_e (h_{aw} - h_w)}$$

(11)

The total enthalpy is defined by the enthalpy at the edge of the boundary layer and the velocity at the edge, and with the rate of heat transfer per unit area, q_w:

$$h_0 = h_\mathrm{e} + \frac{u_\mathrm{e}^2}{2}$$

(12)

and with the heat flux defined as the rate of heat transfer per unit area, q_w,

$$q_w \approx \frac{1}{2} \rho_\infty V_\infty^3 C_H$$

(13)

Drag is defined with free stream conditions, ∞, drag coefficient, C_D, and surface area, S:

$$D = \frac{1}{2} \rho_\infty V_\infty^2 S C_D$$

(14)

3.2 CFD Setup

3.2.1 Geometry and Meshing

Aerodynamic analysis occurred for CFD; the model was built internally with 3D-CAD in STAR-CCM+, utilizing 2-D, trimmed meshing for all cases. For the blunt cone and double cone cases, an axisymmetric model was applied to aid in computational cost. All cases have the free stream conditions outlined in Table *1*, Table *2*, and Table *3* below. A steady state model is used to allow for RANS, time-averaged results. Thermal non-equilibrium ideal gas models various runs

for heat flux into and out of the flow from the bodies' front surfaces. Without the thermal non-equilibrium present, the results would lack the changes in boundary heat flux into the flow, as the models represent conditions where different regions of a system have different temperatures, and their energy exchange processes are not in equilibrium. Lastly, a laminar boundary layer is used as the main focus of this study looks at the boundary and shock layers on the front surfaces of the bodies, specifically the layers' thickness at the stagnation region, while turbulence would be seen further downstream in hypersonic flow.

3.2.1.1 Blunt Cone

An experiment was conducted in the Hypersonic Shock Tunnel (HST) 3, located at the Laboratory for Hypersonic and Shock Wave Research (LHSR) in the Indian Institute of Science. The experiments utilized a test model with a conical skirt, and two variations were tested: one with an uncoated surface and another with a thin chromium (Cr) coating [5].

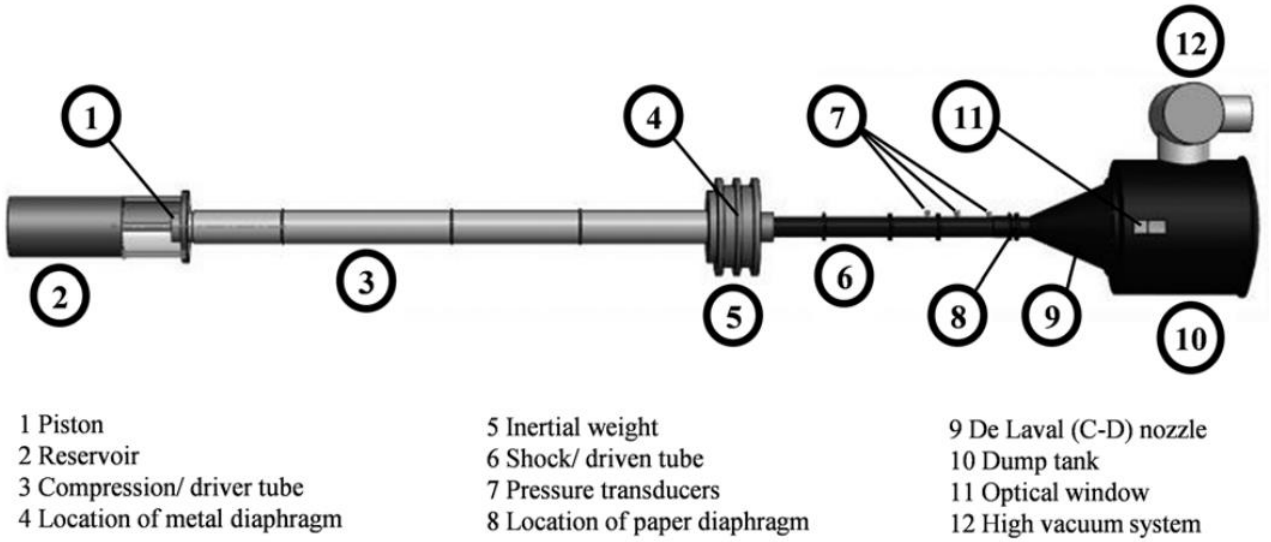

Figure 7: Hypersonic shock tunnel [5]

The test model in experimentation and simulation featured an aluminum (Al) conical skirt with a base diameter of 70 mm and a semi-apex angle of 30◦ that tapered towards the nose with a radius of 30 mm in Figure *8*, referred to as blunt cone.

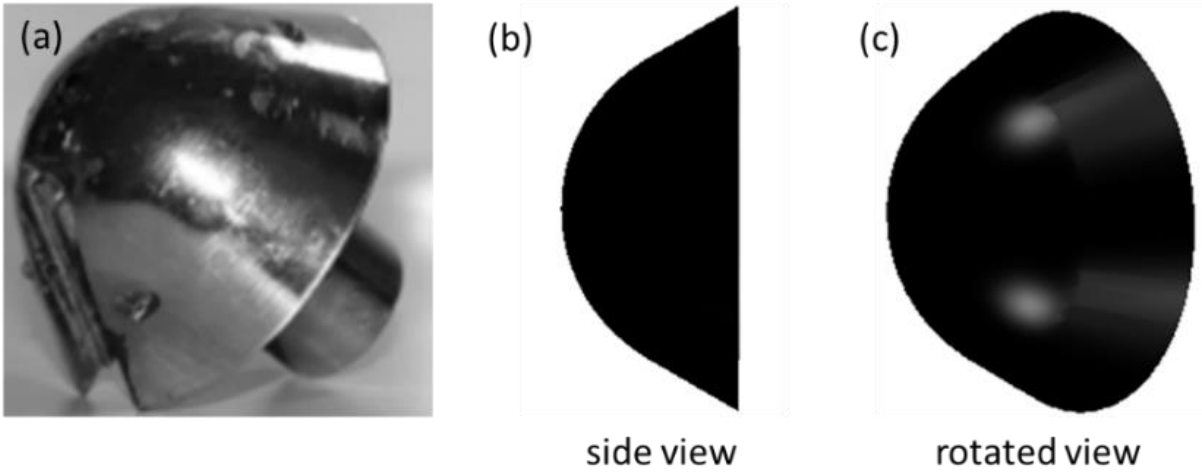

Figure 8: Geometry for large angle blunt cone model with Cr coating for the (a) experiment [5] and (b)(c) CFD

A mesh sensitivity study was conducted to determine the optimal cell isentropic base size. Smaller cell sizes reduce discretization error, but require higher computational time and capacity; therefore, the focus is to select a base size that is as large are possible for while results present all required flow characteristics. Base size varies within a range of 1 mm to 35 mm, as the radius of the blunt cone in the axisymmetric model is 35 mm, and the coarsest mesh option possible. Figure *9* shows the drag converging at 7.0209 N, determined by an infinitely small base size: however, a base size that refined is impossible, as it would calculate with an infinite run time. A reasonable base size is selected to balance the computational capacity with accuracy, 10% of the total geometry base diameter.

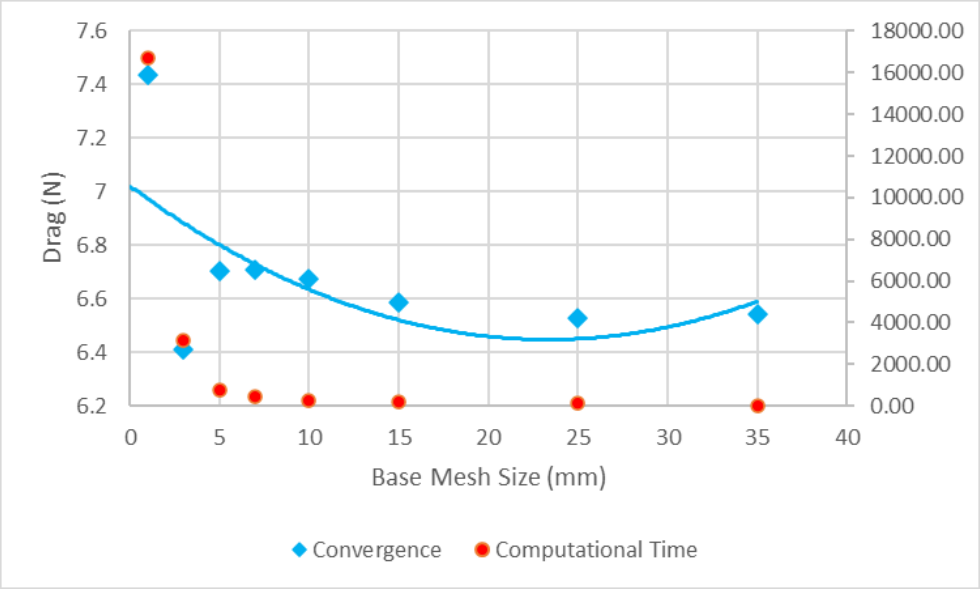

Figure 9: Total drag v. mesh size

As shown in Figure *10*, an isentropic base size of 7 mm was utilized for the axis and bunt cone section and expanded with a growth rate of 1.1. The model has additional refinement, specifically with 8 prism layers with a total thickness of 0.5 mm. A free stream sphere of ~43 times larger than the blunt cone was used for the fluid field, that has far surface control to establish a target base size of 100 mm. This allows for a decreased computational expense as the flow on the edge of the free stream is beyond any aerodynamic effects on the blunt cone. Free stream boundary conditions were applied with the values in Table *1*. Additionally, conical volumetric control with a starting radius of 25 mm to a 100 mm radius around the blunt cone to refine results for the shock and boundary layer, shown in Figure *10* and Figure *11*.

Table 1: Blunt cone free stream conditions [5]

Mach number M_∞ (±1.1%)	9.84
Static pressure P_∞ (Pa) (±2.5%)	200.38
Static temperature T_∞ (K) (±2.2%)	289.68
Static density ρ_∞ (kg/m^3) (±2.1%)	0.0024
Velocity U_∞ (m/s) (±2.1%)	3273
Reynolds number Re_∞ ($\times 10^6$/m) (±6%)	0.43

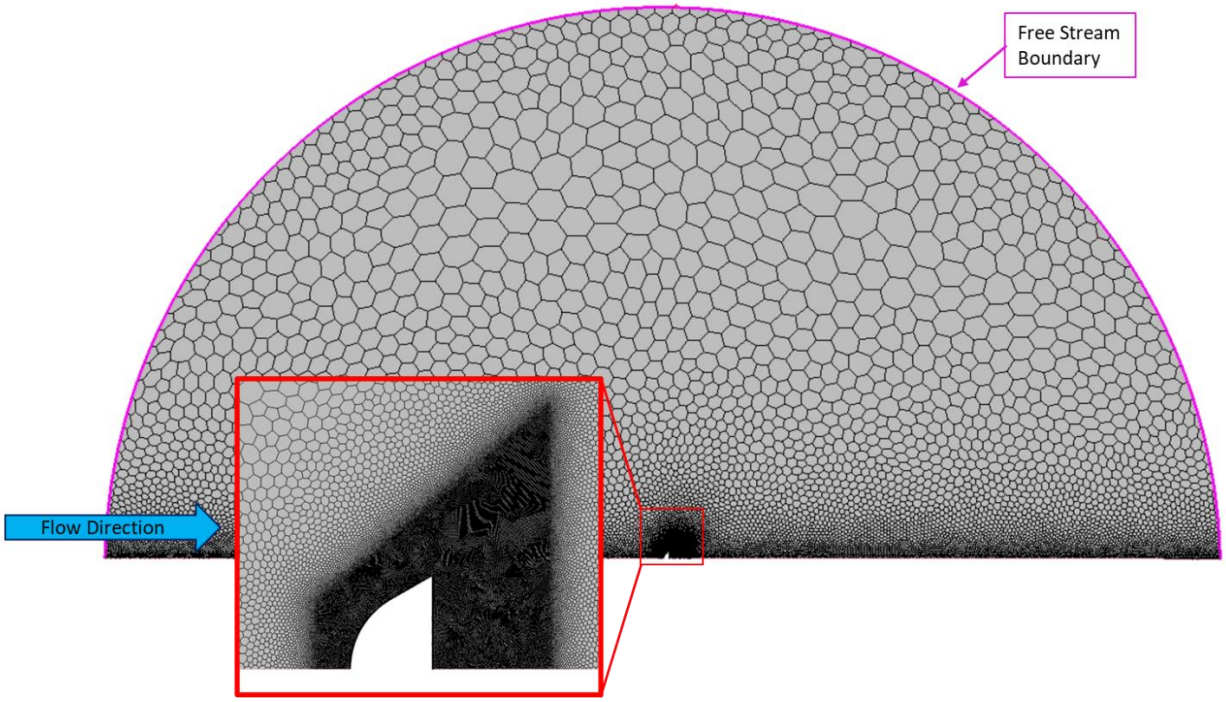

Figure 10: Full view blunt cone 2-D mesh

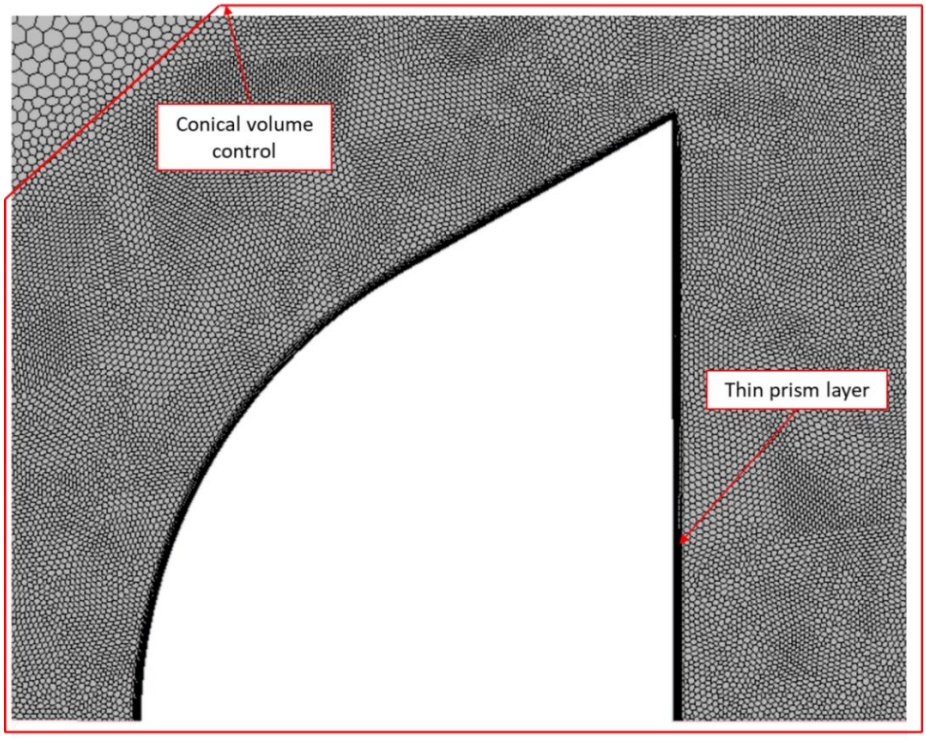

Figure 11: Blunt cone shock layer mesh refinement

3.2.1.2 Double Cone

A sharp, double cone has been studied by CUBRC, and later by Cross and West, consists of a base with diameter 261.85 mm and 50-degree cone, topped with a smaller 25-degree cone with an 85.88 mm diameter as shown in Figure *12*.

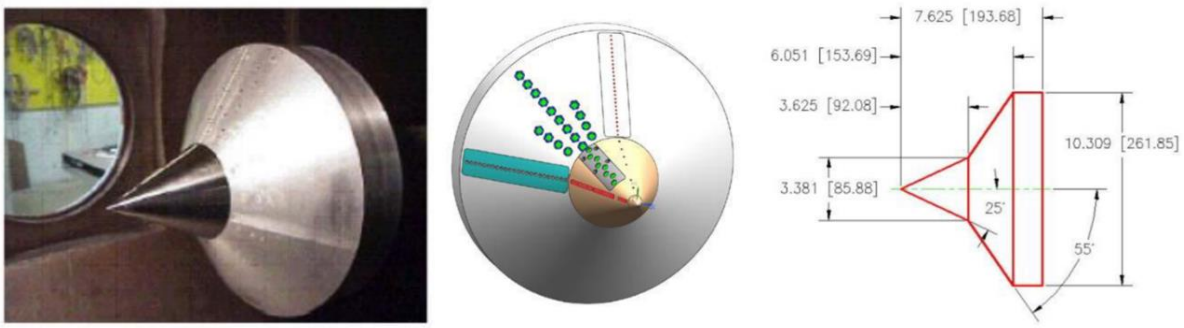

Figure 12: Geometry for 25-/55-degree double cone [8]

Free stream boundary conditions were applied with the values in Table *2*. As shown in Figure *13*, an isentropic base size of 50 mm was utilized for the axis and double cone section and a total prism layer thickness of 5 mm. Settings for surface growth rate, number of prism layers, and free stream surface control remain consistent as the blunt cone and double cone utilizes the same axisymmetric modeling. As shown in Figure *13* and Figure *14*, a conical volumetric control with a starting radius of 300 mm to a 500 mm radius around the body.

Table 2: Double cone free stream conditions [8]

Mach number	10.356	
Static pressure	177.7794	Pa
Static temperature	222	K
Wall temperature	295	K
Velocity	3099.816	m/s

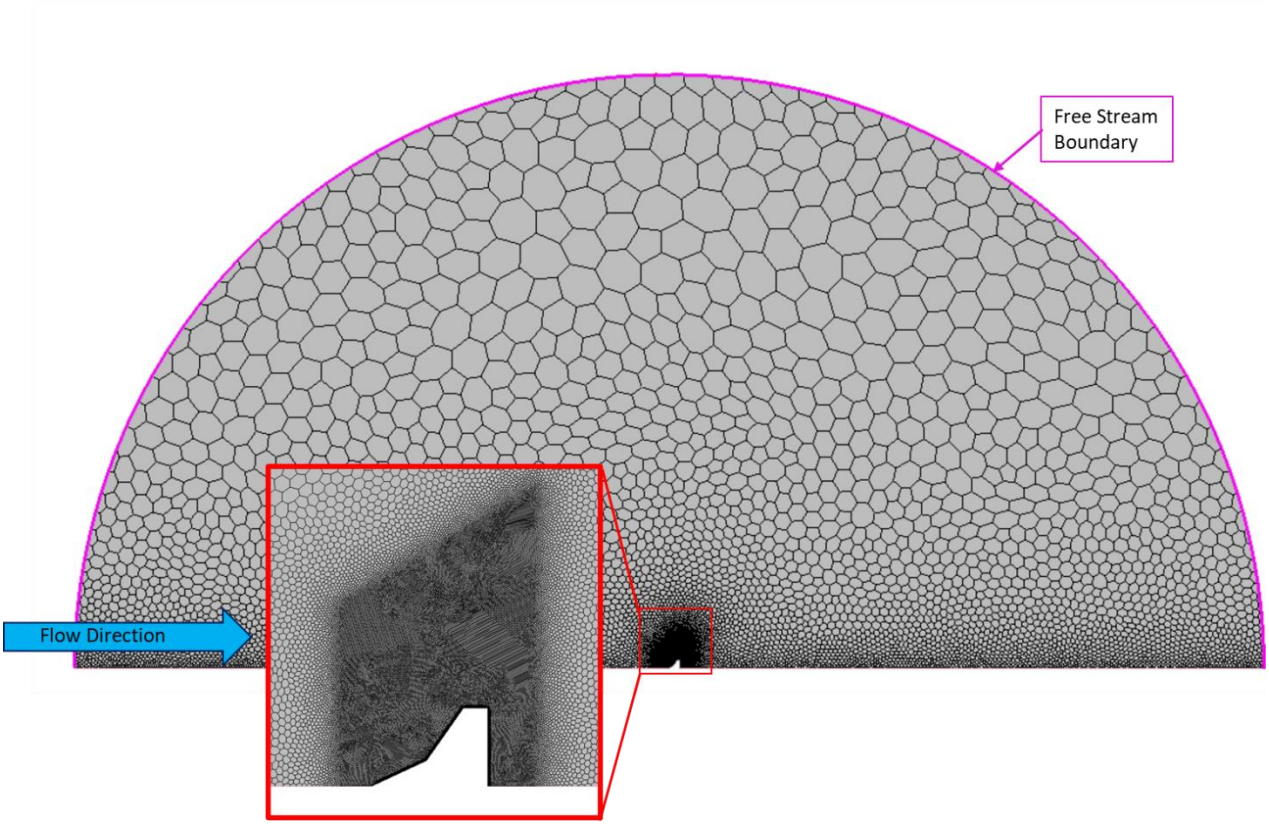

Figure 13: Full view double cone 2-D mesh

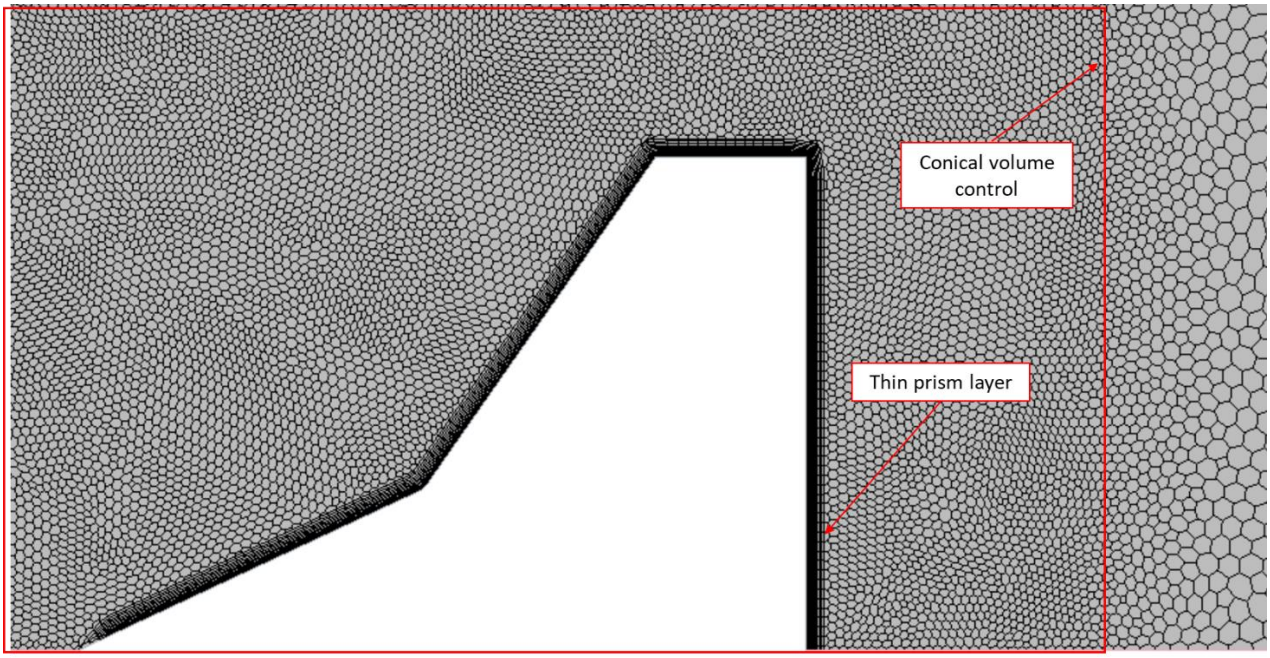

Figure 14: Double cone shock layer mesh refinement

3.2.1.3 Hypersonic Leading Edge

As described by Hernandez et al., the geometry of the hypersonic leading-edge has a 1 mm radius, 5-degree offset and 152 mm chord length.

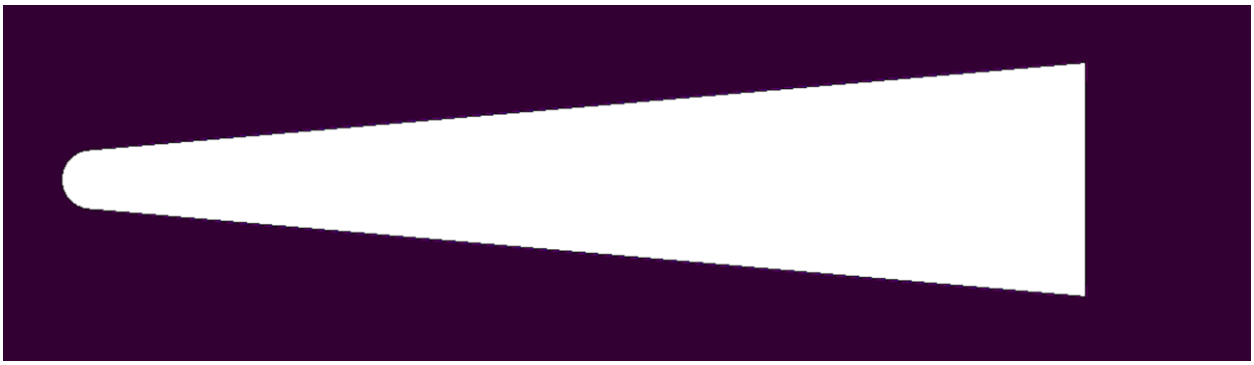

Figure 15: Geometry for hypersonic leading edge [6]

Free stream boundary conditions are outlined in Table *3*. As shown in Figure *16*, an isentropic base size of 500 mm and expanded with a growth rate of 1.3. The model has additional

refinement, specifically with 61 prism layers with a total thickness of 2.5 mm. A free stream block of ~15 times the size of the wedge, with specifically ~12 times the body's length behind the body to capture wake effects; conical volumetric controls separately for the nose and the body set a mesh size of 0.5% of the isentropic base size, shown in Figure *16* and Figure *17*. Free stream boundary conditions were applied with the values in Table *3*.

Table 3: Hypersonic leading edge free stream conditions

Mach number	5	
Static pressure	12110	Pa
Static temperature	217.5	K
Velocity	1475.5	m/s

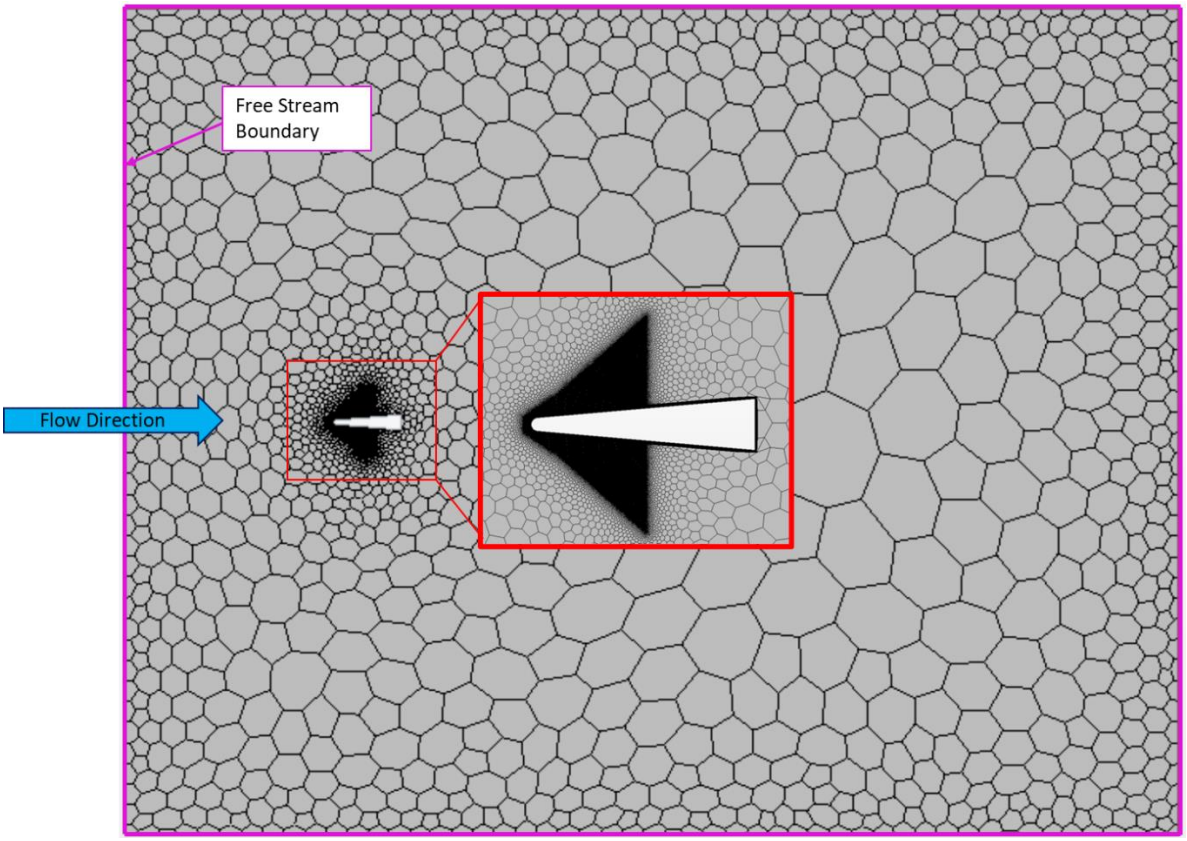

Figure 16: Full view hypersonic leading edge 2-D mesh

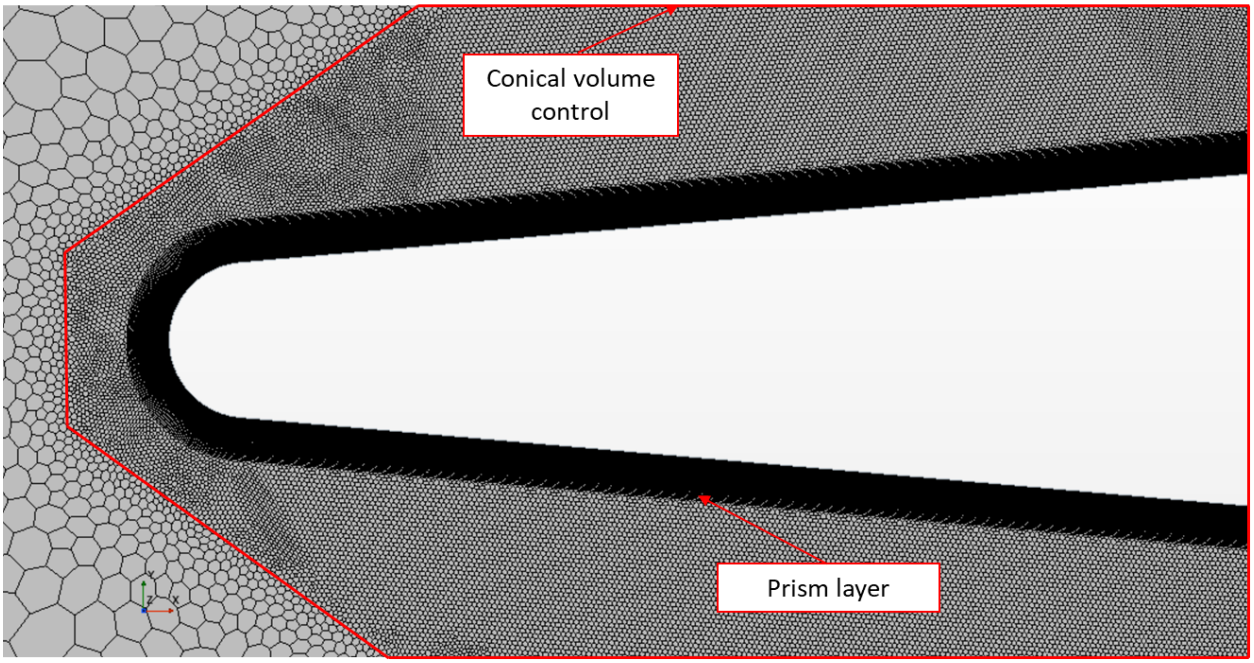

Figure 17: Hypersonic leading edge shock layer mesh refinement

CHAPTER 4: RESULTS AND DISCUSSION

4.1 Effect of Heat Flux

In this study, each of the three geometries were ran under their free-stream and initial conditions for all cases. Initially, cases were run at adiabatic thermal conditions for all boundaries of the flow region, to show the impact of aerodynamic heating alone. Each model had 26 additional cases for a heat flux range of -2,000,000 W/m^2 to 2,000,000 W/m^2, where negative heat flux is out of the flow and positive heat flux is into the flow. Flux was set at the front surfaces of the geometries, excluding the horizontal and base surfaces. Pressure and temperature results for adiabatic, 2,000,000 W/m^2 and -2,000,000 W/m^2 are shown in Figure *18* and Figure *19* respectively. Looking at Figure *18*, the pressure distribution for the blunt cone and hypersonic leading edge are similar between heat flux cases, with little variation. The double cone has a large change from adiabatic conditions when heat is added and removed from the flow. In Figure *18* d, e, and f, the adiabatic flow forms two shocks that share a stagnation point, but adding heat flux causes the boundary/shock layer to push away from the body, while removing heat brings it closer. In Figure *19*, the temperature is directly affected by heat flux for every case; considering heat flux is the energy from heat transfer over the surface area, this is expected. The boundary layer, shock stand-off, and drag are examined to be impacted by temperature and pressure change between cases, and further discussed in the sections below.

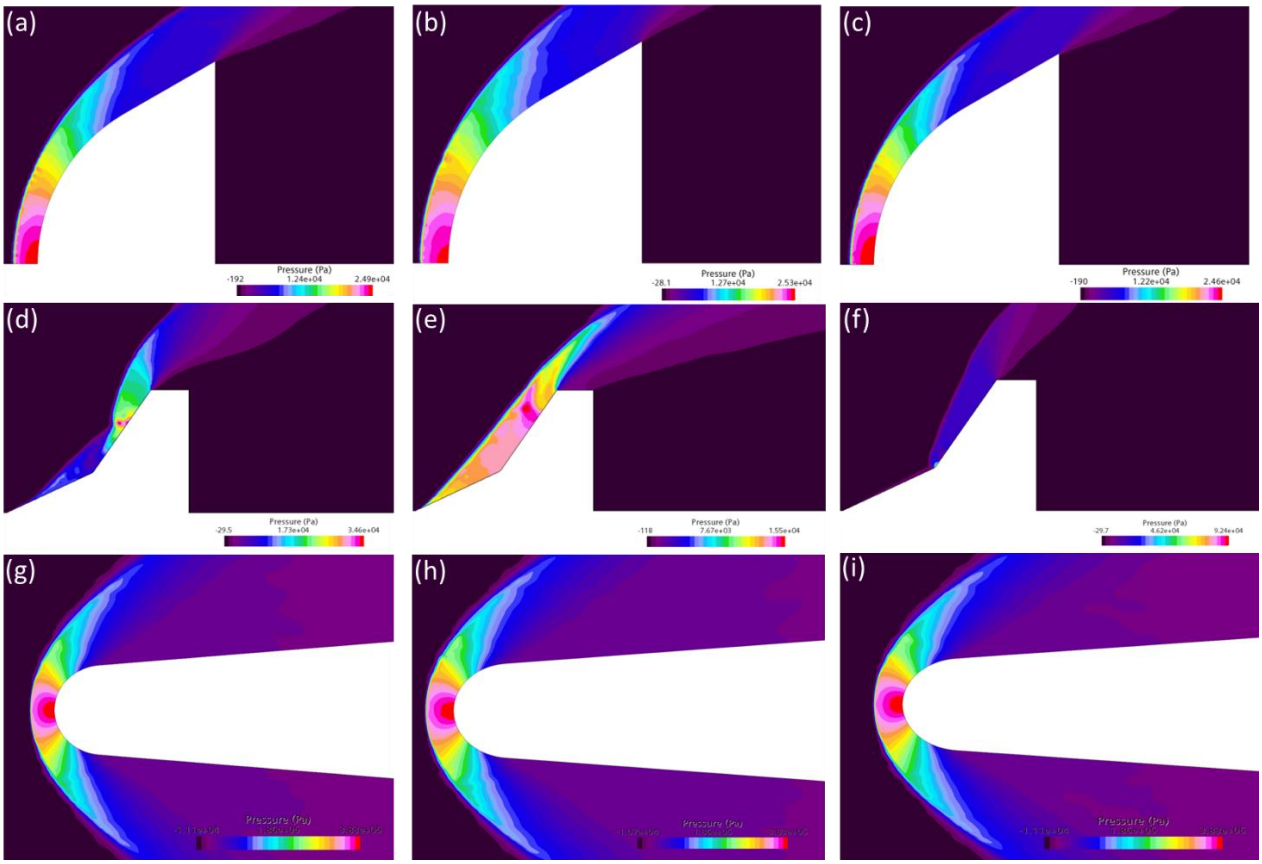

Figure 18: Pressure distribution for the blunt cone at (a) adiabatic (b) 2,000,000 W/m^2 and (c) -2,000,000 W/m^2, double cone at (d) adiabatic (e) 2,000,000 W/m^2 and (f) -2,000,000 W/m^2, and hypersonic leading edge at (g) adiabatic (h) 2,000,000 W/m^2 and (i) -2,000,000 W/m^2

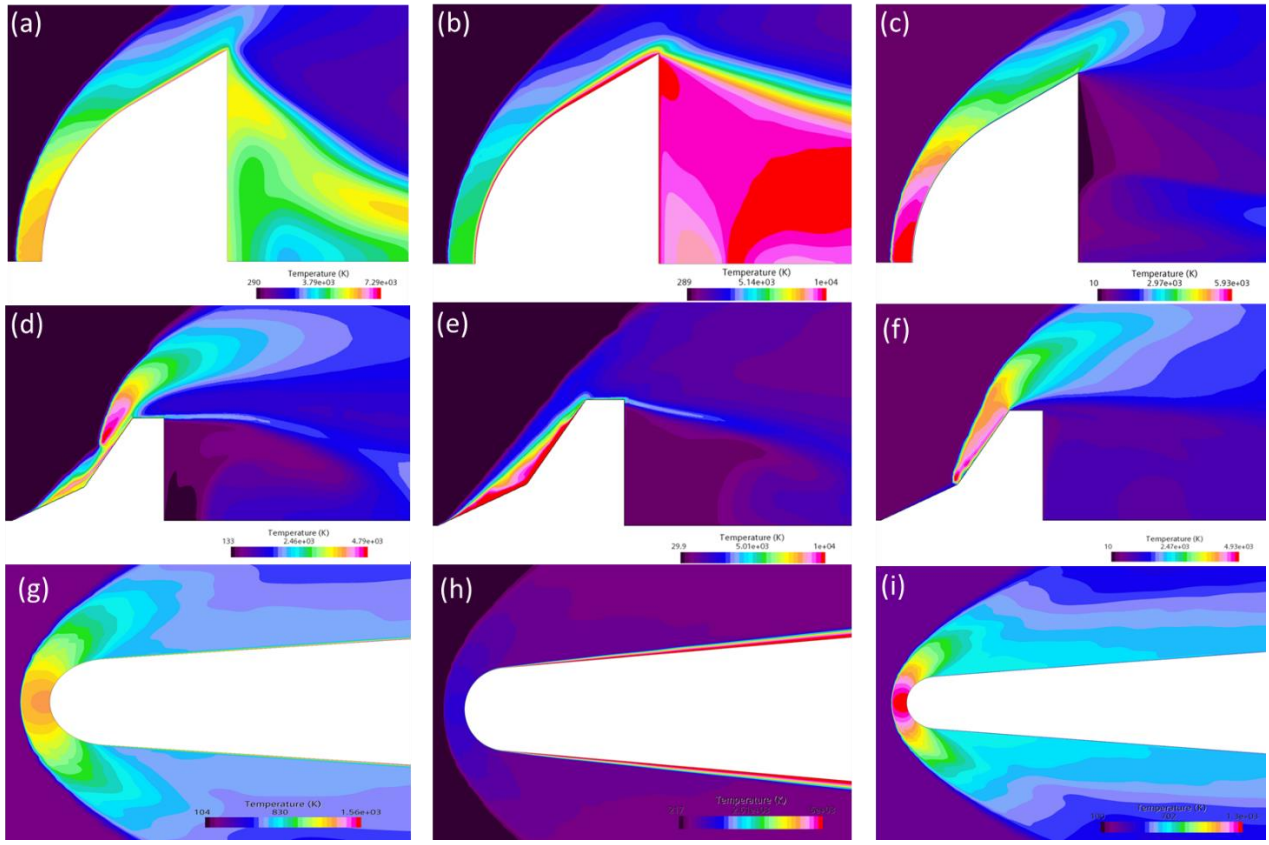

Figure 19: Temperature distribution for the blunt cone at (a) adiabatic (b) 2,000,000 W/m^2 and (c) -2,000,000 W/m^2, double cone at (d) adiabatic (e) 2,000,000 W/m^2 and (f) -2,000,000 W/m^2, and hypersonic leading edge at (g) adiabatic (h) 2,000,000 W/m^2 and (i) -2,000,000 W/m^2

4.1.1 Boundary Layer and Shock Stand-off

As discussed previously, hypersonic flow experiences a thick boundary layer and oblique shocks; therefore, measurements were taken to see how the temperature and pressure change within the boundary and shock layers. Maximum thermal loading measurements were taken at the location shown in Figure *20*; starting at the stagnation points, or location of zero flow velocity, represented by the yellow dot, and a line probe extending from the body represented by the grey dashed line. Boundary and shock layers are both defined by sudden jumps in the pressure/temperature, so points showing those jumps defined the layer thickness. The boundary

layer is the highest-pressure region from the body until the first just, and the shock layer is the second highest pressure region until conditions jump to free-stream values.

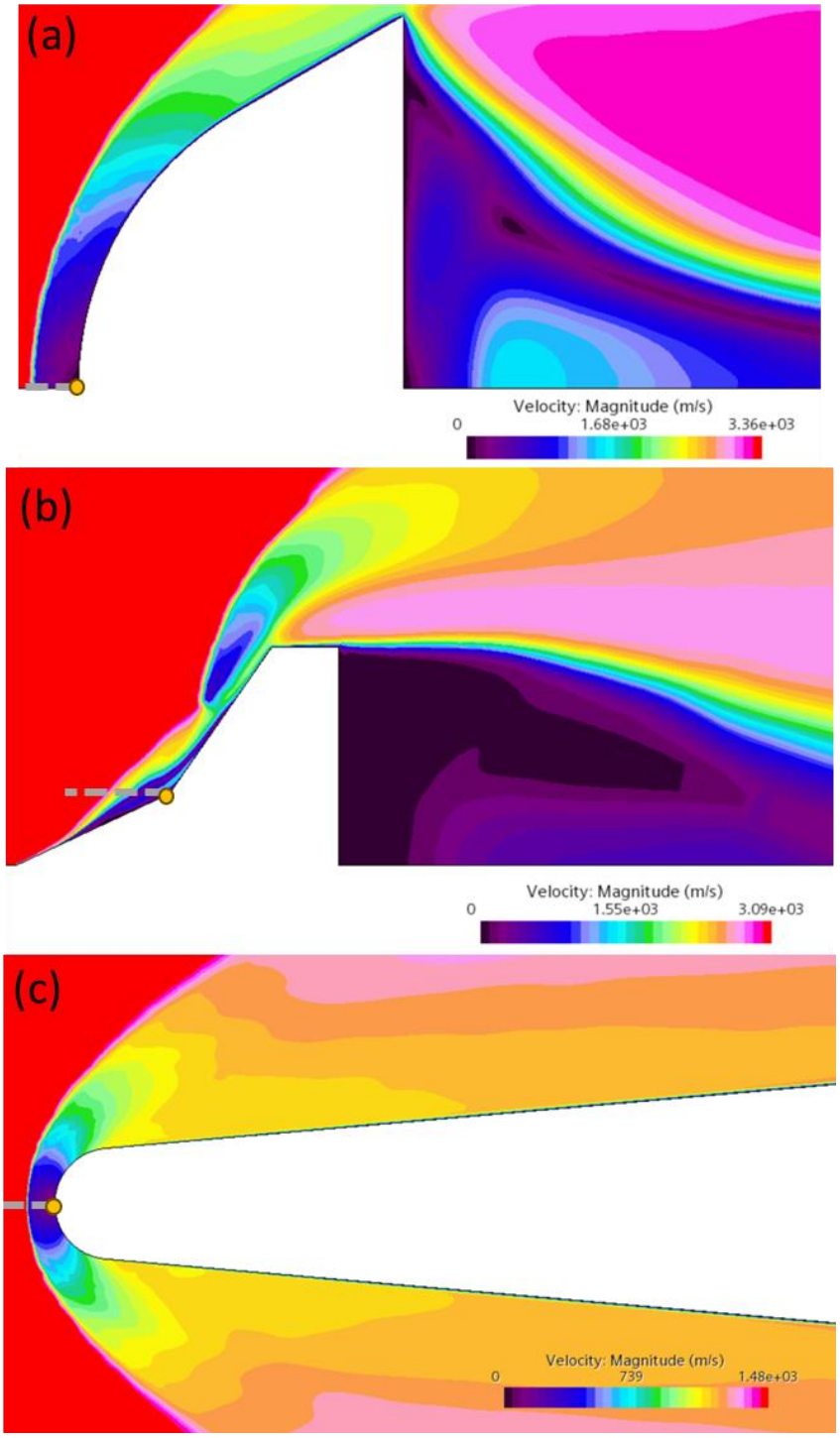

Figure 20: Stagnation point and line probe for (a) blunt cone, (b) double cone, and (c) hypersonic leading edge

For the blunt and double cone cases, the addition of heat flux was influential to the boundary layer thickness and to the shock stand-off distance; however, the hypersonic leading edge did not see an impact on its boundary or shock layer. Figure *21* and Figure *22* shows the pressure and temperature respectively, as a function of the distance into the flow from the stagnation point. Pressure and temperature have a sudden increase across a shock and within the boundary layer; therefore, the drops in the graphs show the transition from the boundary layer at the surface into the shock layer, and then across the shock to the upstream flow. The difference between cases was less than 1.5%, occurring virtually at the same location for all heat flux runs, hence the lack of impact heat flux has on a simpler geometry, like a leading edge.

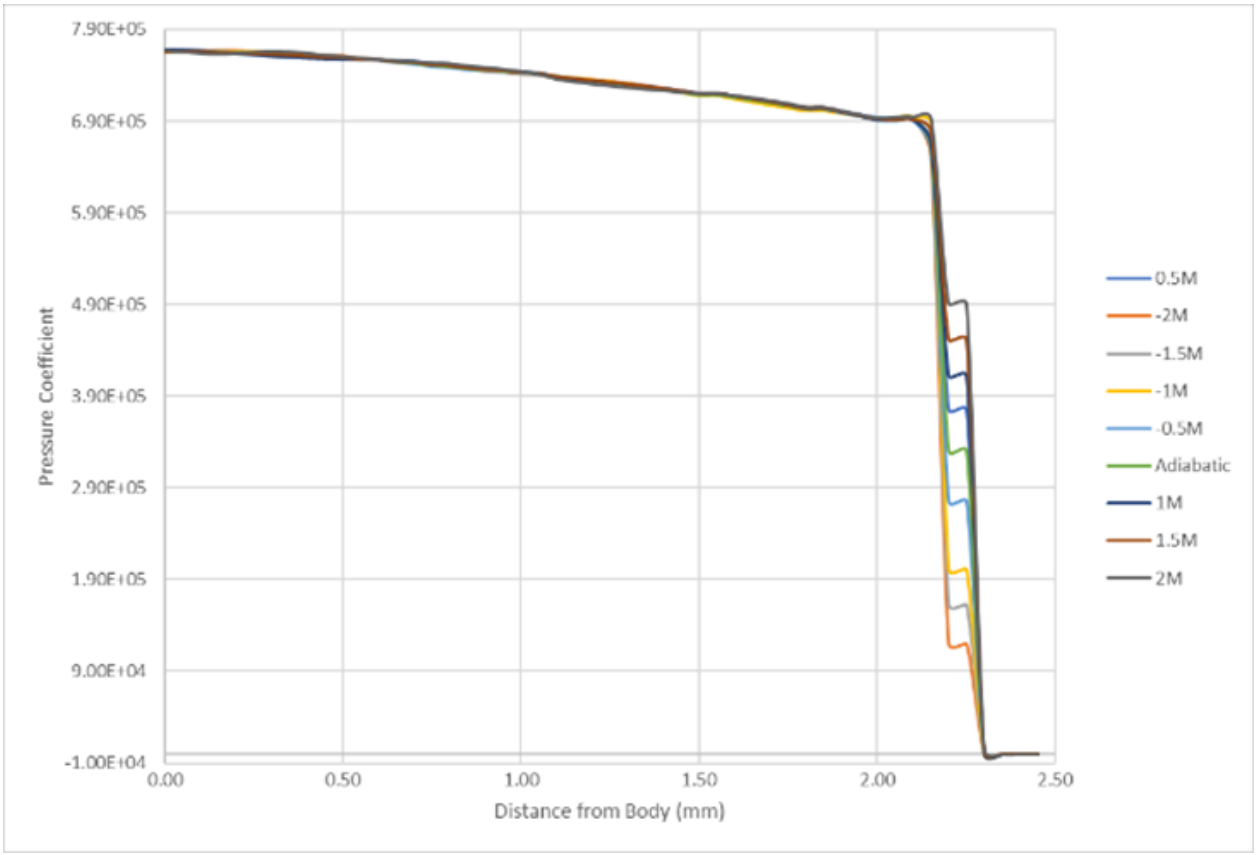

Figure 21: Pressure coefficient v. distance for the hypersonic leading edge surface at the stagnation point

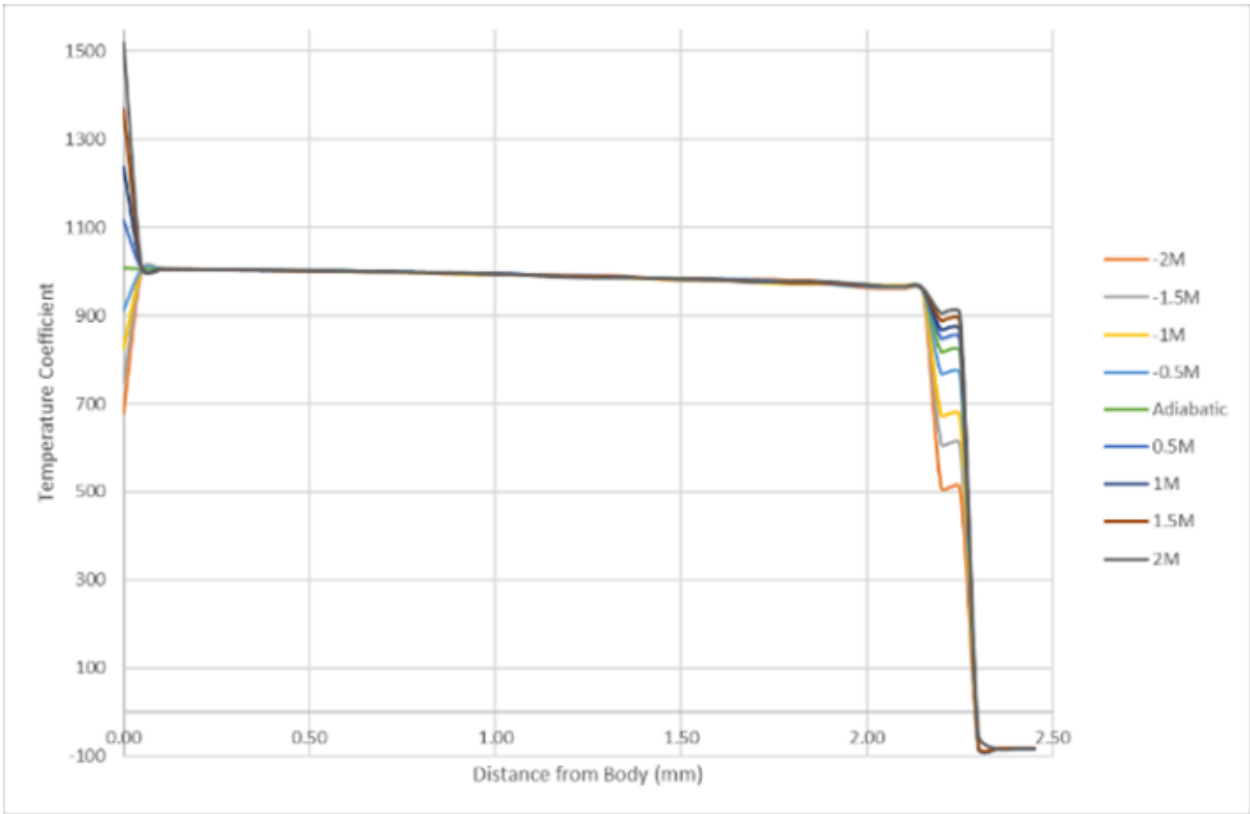

Figure 22: Temperature coefficient v. distance for the hypersonic leading edge surface at the stagnation point

As shown by the value in Table *4*, between the cases of adiabatic flow, -1M W/m^2 and -2M W/m^2 for the blunt cone, there was a 10.26% and 2.74% change respectively for the boundary layer thickness, but the shock stand-off distance saw a 7.06% decrease with the initial addition of heat flux only. For the cases of adiabatic flow, 1M W/m^2 and 2M W/m^2, boundary layer and shock layer saw virtually no change. Looking at the double cone at the same conditions, for heat flux out of the flow, an 180.61% decrease in boundary layer thickness, and a 124.19% and 15.33% difference for the shock standoff distance. For flux into the flow, there's a 40% boundary layer thickness increase, and 15.38% and 3.86% increase in the shock layer.

Table 4: Boundary layer thickness and shock stand-off distance

	Boundary Layer Thickness (mm)			Shock Stand-off Distance (mm)		
Heat Flux (W/m^2)	Blunt Cone	Double Cone	Hypersonic Leading Edge	Blunt Cone	Double Cone	Hypersonic Leading Edge
-2000000	3.6	1.477	2.15	4.1	8.719	2.3
-1000000	3.7	1.477	2.15	4.1	10.167	2.3
0	4.1	28.996	2.15	4.4	43.48	2.3
1000000	4.1	43.48	2.15	4.4	50.722	2.3
2000000	4	43.48	2.15	4.4	52.717	2.3

The boundary layer and shock stand-off were nondimensionalized in Figure *23* for comparison between geometries, dividing the measurements by the geometries' diameter/base length. Additionally, stagnation temperature was normalized in Figure *24*, by dividing the stagnation temperature by the stagnation temperature at adiabatic conditions. The double cone had the greatest thickness at adiabatic flow compared to the other cases shown in Figure *23*, which led to the heat flux having a stronger impact. In Figure *24*, heat flux influences the temperature at the stagnation point for the blunt come the most, but that contradicts the prior conclusion; however, in Figure *25*, the double cone's stagnation pressure is vastly impacted while the other cases see little change. In conclusion, the pressure jump after the oblique shock is the driver for boundary layer thickness and shock stand-off distance.

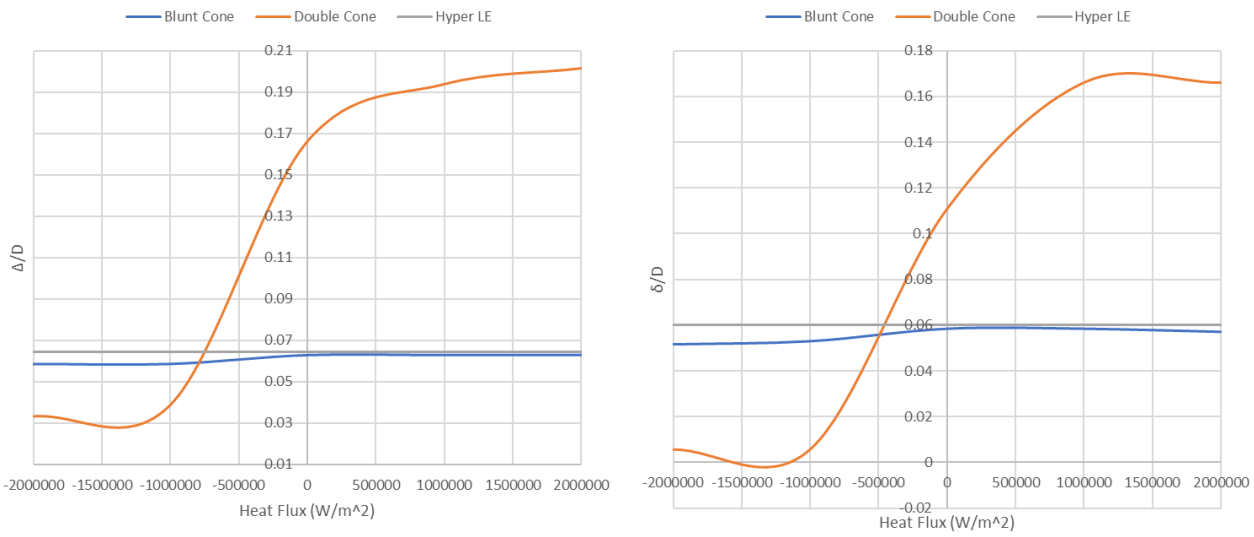

Figure 23: Nondimensionalized boundary layer thickness (δ) and shock stand-off distance (Δ) v. heat flux

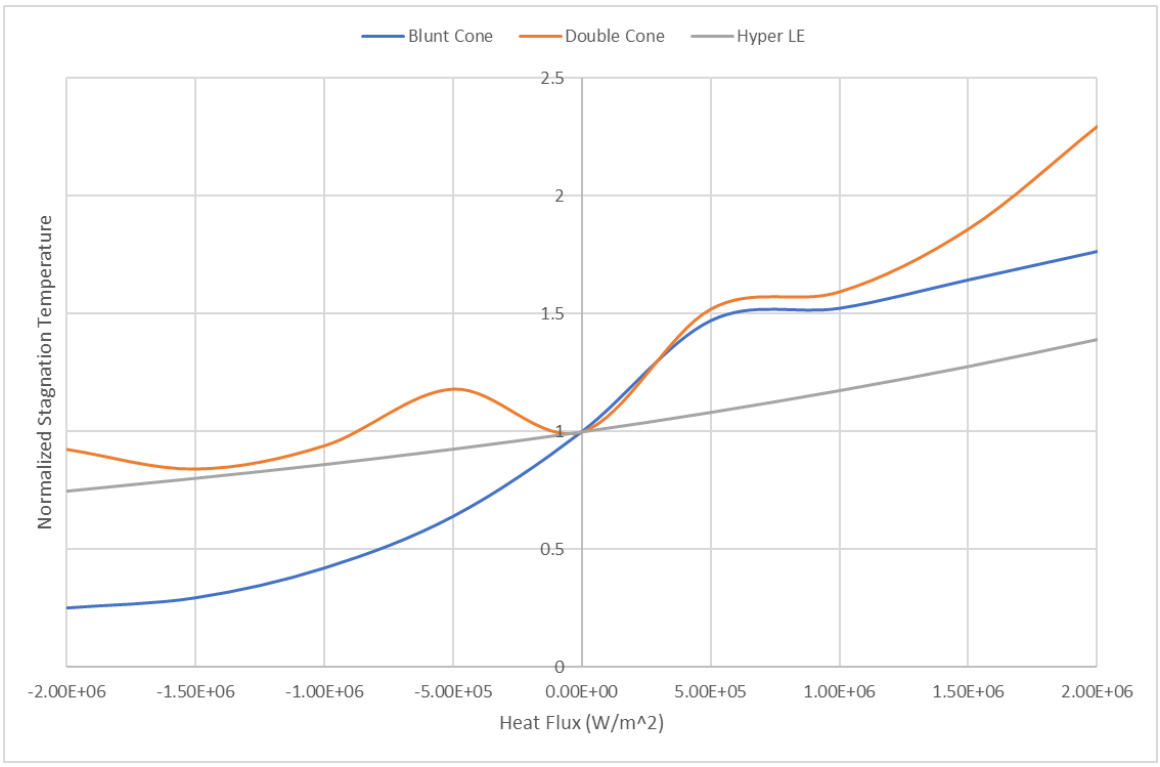

Figure 24: Normalized stagnation temperature v. heat flux

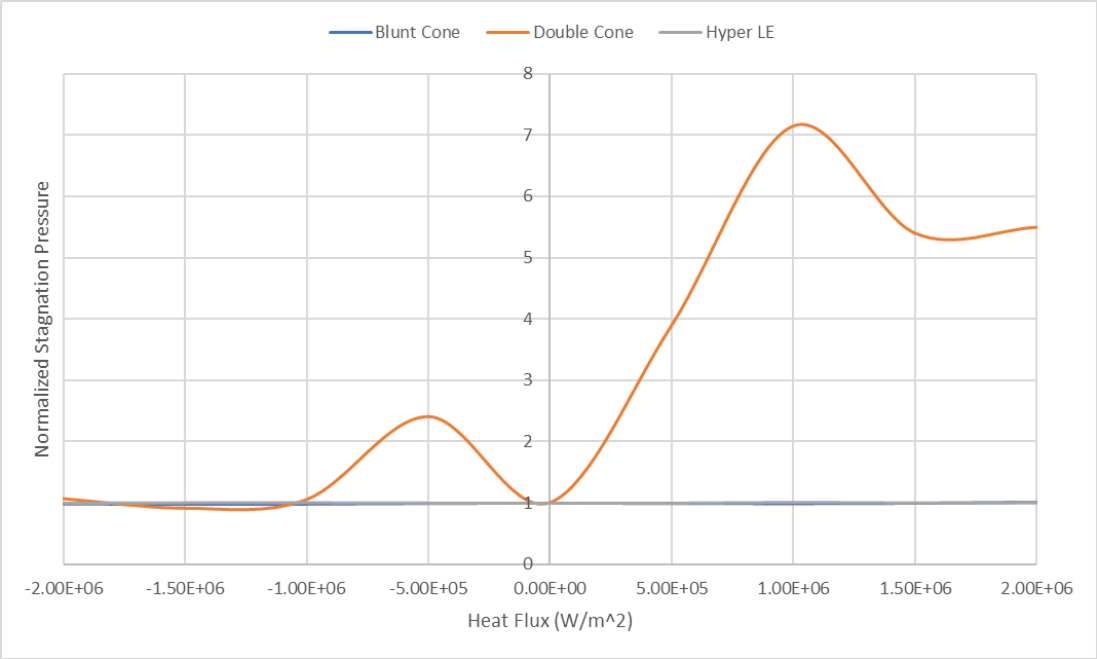

Figure 25: Normalized stagnation pressure v. heat flux

4.1.2 Drag

Each geometry experiences different amounts of drag, as it related to the flow conditions and the geometry itself; however, changing the heat flux also has a direct effect on total drag. Figure *26* displays the drag coefficient for the blunt cone, double cone, and hypersonic leading edge as a function of heat flux. Utilizing drag coefficient helps normalize the data based on the geometry and flow conditions, as those factors can alter results if not considered. Each case is then fitted with a polynomial trendline to examine the overall impact. The hypersonic leading edge drag is divided in half as it is symmetrical across the x axis, and the axisymmetric modeling of the other geometries represent half of the cross section already. At adiabatic conditions, the double cone had a drag coefficient of 0.000218, the lowest compared to the hypersonic leading edge having 0.036127 and the blunt cone having 0.083099. Generally, the presence of a shock wave in hypersonic flow leads to an increase in drag, making it more challenging for the object to overcome

the resistance and maintain its motion through the flow. The double cone had the largest free stream Mach number, but it also has the greatest surface area, this provides an initial assumption that it will have higher drag; however, the results showed the opposite. Figure 18d shows that the front 25-degree cone creates a relatively low pressure jump behind the shock, while the second shock has a larger pressure jump. With two shocks, the double cone has a reduced shock angle for each one. A lower shock angle accounts for a lower overall drag.

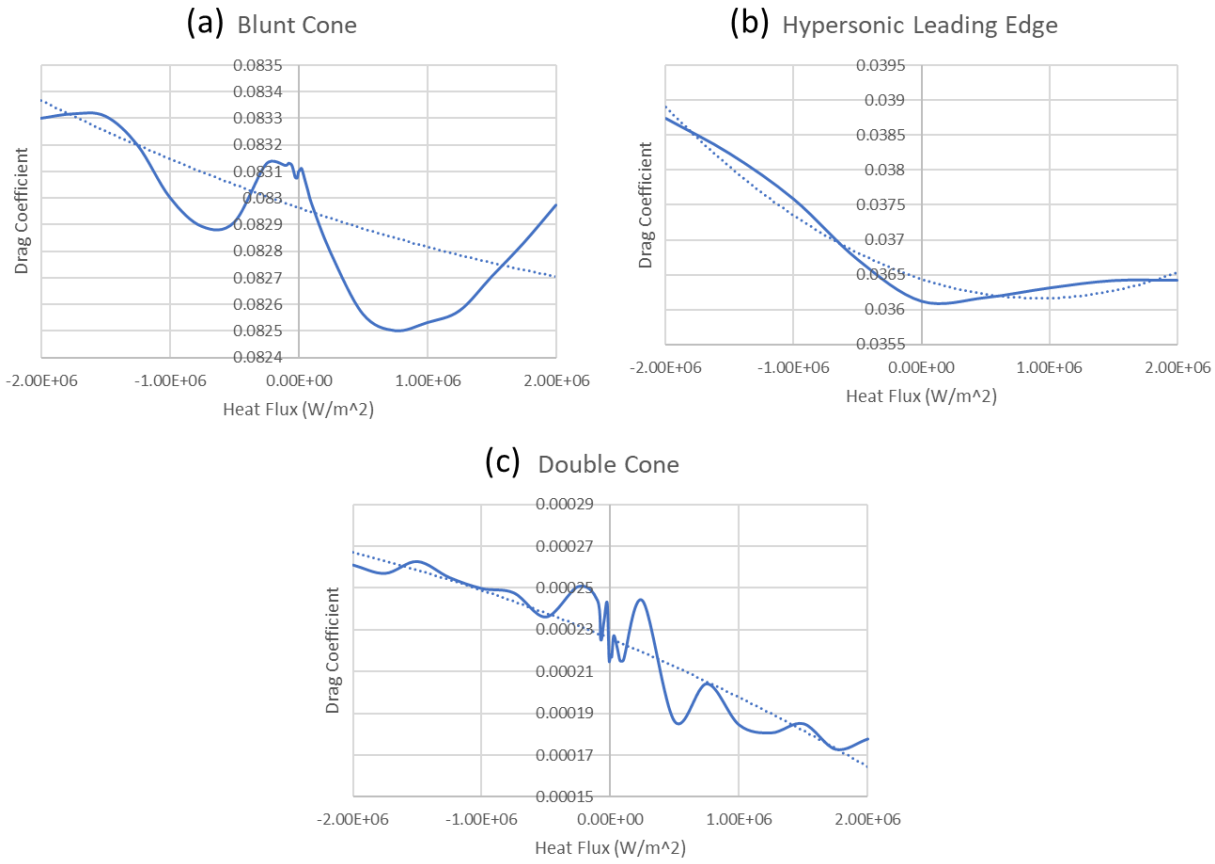

Figure 26: Drag coefficient v. heat flux for the (a) blunt cone, (b) hypersonic leading edge, and (c) double cone

For all cases, adding heat into the flow caused a reduction in drag. As previously discussed, the shock standoff distance increases at the stagnation point causing the flow to change its shape for more complex geometries, such as the double cone. A reduction in drag from adiabatic flow is greatest seen from Figure 18e as the shock standoff is pushed so far out, that the shocks merge to create one large, more aerodynamically efficient shock. In opposition, all cases saw a greater increase in the drag coefficient as heat was removed from the flow. The shock layer being pulled closer to the surface caused the flow to have greater shock angles. As the shock layer moves closer to the surface, the flow encounters higher pressures and temperatures discussed above. These increased conditions lead to a greater deviation of the shock waves from their adiabatic flows, resulting in larger shock angles. The flow becomes more perturbed, and the abrupt changes in pressure and density associated with the shock waves become more pronounced. The abrupt changes in pressure and the disturbances in the flow create additional resistance, requiring more energy to overcome and potentially reducing the vehicle's overall performance and efficiency. The effects observed in a hypersonic flow due to the intense heating experienced by a vehicle highlight the critical importance of managing heat and thermal loads. The impact extends beyond the vehicle's structures and materials to the flow itself, influencing drag forces, flow characteristics, and vehicle performance. Implementing effective cooling methods, such as ablative heat shields, is crucial to protect the vehicle and ensure its safe and efficient operation in hypersonic environments.

CHAPTER 5: CONCLUSION

Aerodynamic heating refers to the transfer of thermal energy from the surrounding flow to the surface of a body moving through high-speed flow. This is particularly relevant in hypersonic flight conditions, where the flow velocities are beyond Mach 5 and result in intense heating of the vehicle surfaces. Understanding heat flux in the context of aerodynamic heating is essential for several reasons as it allows for the prediction and assessment of the thermal loading experienced by the vehicle surfaces, its impact on the structural integrity and performance of the vehicle, but also to understand the changing in the energy within the flow itself. Within the flow, there are shocks and characteristics changing in greater ways than predicted at supersonic speeds. At the stagnation point of a hypersonic flow, the maximum thermal loading occurs so we base comparisons of temperature, pressure, shock/boundary layer thickness, and drag at that location. By analyzing the temperature and pressure, we determined the distances between the shock wave and the boundary layer and observe how the addition of heat flux will push them further away from the body, and removing heat flux does the opposite. This change is particularly evident in the more complex geometries. As seen in the double cone, where two shocks are observed in adiabatic flow; however, as the heat flux increases, the shock layer is pushed even further from the body, eventually causing the shocks to merge and have one larger shock angle acting to turn the flow less than two smaller angles. This merging leads to a reduction in drag across the body, resembling the behavior of an ablative heat shield that is oxidizing or burning into the flow. Understanding the impact of heat flux on the flow characteristics, such as shock and boundary layer distances, is crucial for designing efficient hypersonic vehicles. It allows engineers to optimize the geometry, consider cooling mechanisms, and potentially exploit heat flux as a means of enhancing aerodynamic performance.

REFERENCES

[1] R. A. East, J. A. E. “HYPERSONIC MISSILES – SOME AEROTHERMODYNAMIC PROBLEM AREAS.” 2000.

[2] Half, J. L., Noca, M. A., and Bailey, R. W. *COST-BENEFIT ANALYSIS OF THE AEROCAPTURE MISSION SET*.

[3] Lockwood, M. K. *AIAA 2003-4799 TITAN AEROCAPTURE SYSTEMS ANALYSIS*. 2003.

[4] John D. Anderson Jr. *Hypersonic and High-Temperature Gas Dynamics, Second Edition*. 2006.

[5] Deep, S., and Jagadeesh, G. “Aerothermodynamic Effects of Controlled Heat Release within the Hypersonic Shock Layer around a Large Angle Blunt Cone.” *Physics of Fluids*, Vol. 30, No. 10, 2018. https://doi.org/10.1063/1.5046191.

[6] Hernandez, J., Fouliard, Q., Anderson, C., Northam, M., Vo, K., Clabaugh, J., Wolfe, D., Almer, J., Park, J., Ghosh, R., Gou, J., Kinzel, M., and Raghavan, S. In-Situ XRD Characterization of Interface Strains In Multilayered Ceramic Composite Systems for Hypersonics Applications. 2020.

[7] Siemens. STAR-CCM+ Users Manual .

[8] Cross, P. G., and West, M. R. *Simulation of Hypersonic Flowfields Using STAR-CCM+*. 2019.